A Numerical Study of the Effect of Aggregate Fracture on the Unbound Granular Materials Response under Triaxial Loading

M. K. Etikan, D. Jelagin, M. N. Partl
KTH Royal Institute of Technology, Stockholm, Sweden

E. Olsson
Luleå University of Technology, Luleå, Sweden

ABSTRACT: The performance of unbound granular materials (UGMs) made from crushed rock plays a critical role in the service life of roads. While experimental evidence indicates that aggregate crushing and abrasion significantly affect UGM stiffness and permanent deformation, the precise relationship between aggregate strength and UGM performance remains unclear. This is particularly important when using aggregates of marginal strength in road construction. This study investigates the impact of aggregate breakage on UGM behavior under triaxial loading, using the Discrete Element Method (DEM) for computational analysis. The model examines how aggregate breakage influences UGM response for two different types of aggregates. The DEM results are compared with experimental data from the literature. Findings show that particle fracture significantly influences the maximum deviatoric stress that the UGM can endure under two different confining pressures, highlighting the importance of aggregate strength in determining UGM performance.

1 INTRODUCTION

Unbound granular materials (UGMs) composed of crushed rock are extensively used in road construction. Their performance in unbound road layers has a profound effect on road's service life. A considerable number of experimental, numerical and field studies have thus been performed to clarify the relationship between UGMs' material parameters and their mechanical behavior with respect to their stiffness and resistance to permanent deformation. In particular, the influence of UGM gradation has been extensively studied, e.g. (Yideti, et al., 2013; Erlingsson & Rahman, 2013). There is also strong experimental evidence that adequate resistance of aggregates to crushing, and abrasion is crucial for UGM performance, as aggregate breakage may significantly increase permanent deformation accumulation rates and compromise stiffnesses of UGMs (Saeed, et al., 2001). A quantitative relationship between the strength of the aggregates and UGM performance is however not fully understood yet. This issue is particularly important with respect to incorporating marginal aggregates in road UGMs (Zhang, et al., 2021). This study seeks to contribute to clarifying this issue, by investigating computationally the effect of aggregate breakage on the UGM performance under triaxial loading.

Etikan et al. (2024) proposed recently a new Discrete Element Method (DEM) modelling framework to model the aggregate breakage in UGMs. The framework was shown to capture accurately the effects of aggregate gradation, fracture toughness and load level on aggregate crushing in UGMs subjected to uniaxial compressive loads. Presently, the modelling approach is extended to triaxial loading conditions and the DEM prediction are compared to the experimental results by Rahman & Erlingsson (2013). The developed model is used to investigate the influence of aggregate breakage on UGM response to triaxial loading for two different aggregate types.

2 COMPUTATIONAL METHODOLOGY

2.1 *DEM Modelling*

DEM modelling is employed to evaluate the effect of aggregate fracture in UGMs under monotonic triaxial tests. The model is implemented using commercial software, PFC3D^{TM} (Itasca Consulting Group Inc., 2019) where contact and statistical fracture force models are incorporated as subroutines as presented below in Sections 2.2 and 2.3. The aggregates are represented as spherical particles in DEM. In what follows the particles used in experiments will be referred to as "aggregates", whereas the those employed in DEM will be designated as "particles". The interlock effect in UGM is applied by constraining the rotation of particles. Each particle is characterized by its density, stiffness, toughness, size, friction (μ) and damping (η) coefficients. The model geometry is illustrated in Figure 1a along with the loading and boundary

conditions used. The boundary of the system is generated by the confining cylinder which consists of three components. The radial wall represents latex membrane with a shear modulus of 1 GPa as implemented by de Bono & McDowell (2014), while the horizontal top and bottom walls represent the loading head and the pedestal respectively. The velocity, u, of the bottom wall is zero through the simulation. Top and bottom walls are assigned a stiffness 200 times higher than the particles to represent rigid bodies. The friction between the confining cylinder and particles is set to zero.

In DEM model, particles are generated randomly within the confining cylinder space, and gravity is applied to allow them to fall. Next, the loading head is placed on top of the UGM, and the UGM is compressed from both the radial wall and the loading head until the designated confining stress, σ_C, is reached. The confining stress is calculated for each wall as the sum of the forces arising from particle-wall contacts, divided by the area of the respective wall. Finally, the UGM is compressed in displacement control mode, while maintaining the confining stress on the radial wall at designated σ_C. The deviatoric stress, σ_d, is calculated as the difference between the stress applied on the loading head and the confining stress.

The position and the velocity of each particle are calculated through explicit numerical integration of Newton's laws of motion. The external forces acting on the particles are generated by gravity and through interactions with other particles or walls. Furthermore, the velocity of each accelerating particle is affected by η, as introduced by PFC3D^{TM}, where it can take any value between 0 and 1. It allows particles to reach a steady state after falling due to gravity. It affects the applied force on particles as $F - F_\eta = ma$, where F is the force applied on a particle, and m and a represents the mass and the acceleration of the particles respectively. $F_\eta = F\eta$ is the damping force.

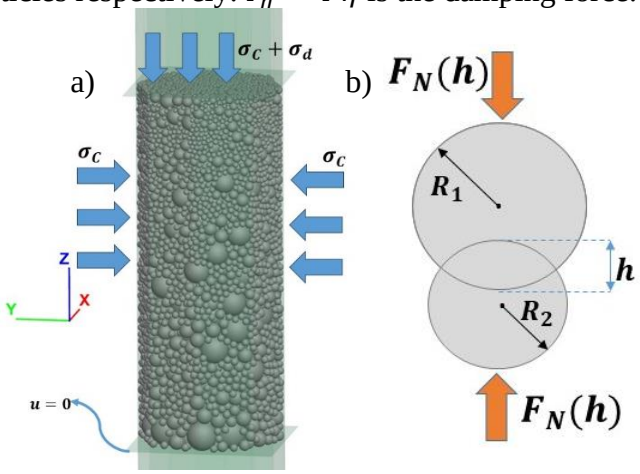

Figure 1. a) DEM model of UGM at σ_C = 10 kPa and σ_C = 0, b) Overlapping of two particles in contact.

2.2 *Contact Model*

The normal contact between two particles is illustrated in Figure 1b. The contact force model applied in this study was developed by Olsson et al. (2019a), based on the experimental results from Cervera et al. (2017). The normal contact force, F_N, is derived as a function of overlapping, h, between particles, and their relation is expressed in three stages, as shown in Eq. (1). The first stage represents the crushing of surface asperities where the relation between h and F_N is observed to be linear until the depth of surface asperity, h_s. Subsequently, F_N follows Hertz contact theory until the indentation depth h_L, which corresponds to the onset of shear driven damage, resulting in linear relation between F_N and h. The values of h_s and h_L are reported as 0.02 and 0.08 mm, respectively (Cervera, et al., 2017). This result in the following normal contact model:

$$F_N = \begin{cases} (F_S/h_S)h, & h \le h_s \\ k_p\,(h-h_1)^{1.5}, & h_s \le h \le h_L \\ k_p\,(h_L-h_1)^{1.5} + 1.5\,k_p\sqrt{h_L-h_1}\,(h-h_L), & h_L \le h \end{cases} \quad (1)$$

where F_s = 100 N (R_0 / 6.25 mm)$^{0.5}$. The effective contact radius is denoted as $R_0 = (1/R_1+1/R_2)^{-1}$ where R_1 and R_2 represent the radius of the overlapping particles, and $h_1 = h_s - (F_s/k_p)^{2/3}$. The contact stiffness is k_p, and given by Hertz (1882) contact theory as follows:

$$k_p = (2/3)E_{eff}R_0^{0.5} \quad (2)$$

where the effective Young's modulus between particles in contact is represented as $E_{eff} = ((1-\nu_1^2)/E_1 + (1-\nu_2^2)/E_2)^{-1}$, with $E_{1,2}$ and $\nu_{1,2}$ denoting the Young's modulus and Posson's ratio of the particles in contact, respectively.

2.3 *Statistical Fracture Force Models and Fragmentation Modelling*

To be able to acquire an accurate fracture response, the assessment of these critical fracture forces, F_f, is essential. The fracture forces are assigned based on a Weibull weakest link approach that accounts for two sources of variability in aggregates strength: size dependency and aggregate shape. The cumulative density function for critical fracture forces, S, is presented in Eq. (3).

$$S = 1 - \int_{R_N}^{R_{N+1}} \int_0^\infty p(\xi)p(R)e^{-\left(\frac{F_f}{\sigma_W R^2}\xi\right)^m \frac{R^3}{V_{ref}} I_0 d\xi\, dR} \quad (3)$$

where σ_W and m are the material parameters, and R_N and R_{N+1} represent the half of smaller and larger size respectively. The reference volume, V_{ref}, is introduced for dimensional consistency. The stress distribution within an aggregate is presented as $\sigma(\mathbf{x})$. The probability distribution for the particle size, $p(R)$, and for particle shape, $p(\xi)$, are given by:

$$p(R) = \frac{2R_N^2 R_{N+1}^2}{(R_{N+1}^2 - R_N^2)R^3} \quad (4)$$

$$p(\xi) = \frac{n}{I_0}\xi^{n-1}\exp[-\xi^n] \quad (5)$$

where n controls the scatter of the fracture force distributions, I_0 determines the median value of I which represents the stress state of an aggregate as shown:

$$I = \int_{\tilde{V}} \tilde{\sigma}(\mathbf{x}) d\tilde{V} \quad (6)$$

where $\sigma(\mathbf{x}) = \tilde{\sigma}(\mathbf{x}) F_f / R^2$ and $V = \tilde{V} R^3$ are the normalized variables.

The particle will fracture when F_N exceeds F_f for a given contact pair. Once this condition is met, the Young's modulus of the particle is reduced according to $E_{fractured} = C_W E_{initial}$, where C_W is a weakening coefficient, and $E_{initial}$ and $E_{fractured}$ denote the Young's modulus of the particle before and after fracture, respectively. The range of C_W is between 0 and 1. This coefficient is applied to simulate the local settling that occurs after a particle fractures. According to Eq. (3) – (6), the distribution of F_f is defined by three material parameters: σ_W, m and n. While post-fracture behavior of the particle is defined by C_W.

3 COMPUTATIONAL STUDY

The model presented in the previous section is used to simulate the monotonic triaxial tests conducted by Erlingsson & Rahman (2013) on UGMs composed of high strength gravel aggregates, referred to as SG1. Contact and fracture force model parameters, i.e. $E_{initial}$, C_W, density,ρ, Poisson's ratio, ν, σ_W, m and n are identified following Etikan et al. (2024, 2025) and presented in Table 1.

Table 1. Parameters of contact and fracture force models.

$E_{initial}$	C_W	σ_W	m	n	ν	ρ
GPa	-	MPa	-	-	-	g/cm^3
45	0.3	76.04	4.69	5.07	0.15	2.65

The SG1 UGM used by Erlingsson & Rahman (2013) was compacted to cylindrical confinement with a volume of 5.3 L, 150 mm diameter and approximately 300 mm height.The gradation of the UGM followed the theoratical Fuller curve, $G_V = (d/d_{max})^{0.5}$, where d represents the aggregate size, d_{max} is the maximum aggregate size and G_V is the cumulative volume distribution. The gradation curve of SG1 is presented in Figure 2 along with the particle size distribution used in DEM simulations. As may be seen, in simulations a cut-off is introduced at 4 mm for computational effiency. The volume of particles smaller than 4 mm is distrubuted proportionally to other sieve sizes. The porosities of the UGM in the experiments and simulations are 19% and 34% respectively.

In DEM model, particles are generated uniformly between 4 and 31.5 mm. Total of 9208 particles are generated. To achieve the densest particle arrangement in DEM, particles are generated in 10 layers with the initial condition of μ = 0 and η = 0.1. Once particles are settled on the bottom of the cylinder, μ is set to 0.7, following Olsson et al. (2019a) and Etikan et al. (2024). Two levels of confinement stress, σ_C =10 and 20 kPa are simulated. For each σ_C the simulations are conducted with and without particle breakage, in order to examine the effect of breakage on UGM performance. Furthermore, for $\sigma_C = 20$ kPa, triaxial test is also conducted with fracture force model parameters adjusted to represent marginal aggregates: m=6.51, σ_W=15.5 MPa and n=1.67 are used, corresponding to the ones measured for relatively weak granite aggregate by Etikan et al. (2025).

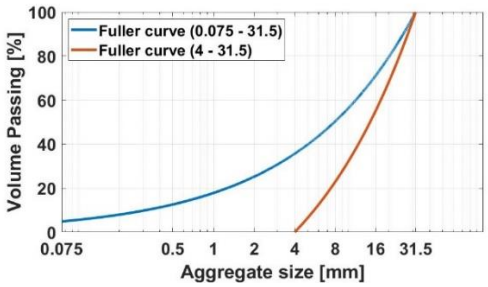

Figure 2. Gradation used in experiments and in DEM model.

4 RESULTS AND DISCUSSION

The simulation results of monotonic triaxial tests compared to experimental results by Erlingsson & Rahman (2013) in Figure 3, where σ_d is show as a function of UGM's vertical strain, ϵ_Z. Firstly, it may be seen that experimental and modelling results exhibit qualitatively similar behaviors. The measurements reach the maximum σ_d at approximately 1.1 and 1.2% of strain for σ_C = 10 and 20 kPa respectively. The corresponding simulation results, both with breakage and without breakage, deviate no more than 0.1% from the measurements. However, the simulation results of the maximum σ_d and stiffness values show some discrepancies with the measurements. Specifically, the UGM stiffnesses at the initial portion of the test are below the ones predicted computationally. For σ_C = 20 kPa models, the maximum σ_d is 1.5 and 1.3 times higher in the UGM with strong and weak fracture resistance simulations, respectively. In contrast, the simulation results for σ_C = 10 kPa align with measured maximum σ_d. Some quantitative deviations are expected however given the differences in porosity between the experiments and simulations, as well as possible deviations of particle breakage characteristics for the aggregates used Etikan et al. (2024, 2025) and Erlingsson & Rahman (2013) studies. The qualitative agreement observed in Figure 3 is encouraging however, and quantitative agreement may be improved by adjusting contact and fracture model parameters to account for the effect of finer particles not modelled explicitly in DEM. This will be addressed in future research.

The main interest of this study is to evaluate the effect of particle fracture in triaxial testing. As shown in Figure 3, particle fracture in both confining cases

results in a decrease in the maximum σ_d that the UGM can withstand. This decrease is approximately 3.5% for each respective confining case of UGM with strong fracture resistance and 12.3% for UGM with weak fracture resistance. The effect of fracture is particularly evident in σ_C = 20 kPa model with weak resistance to fracture. Additionally, DEM simulations enable tracking particle fractures, allowing for the observation of fracture locations within the UGM and the corresponding σ_d, as shown in Figure 4 and 5.

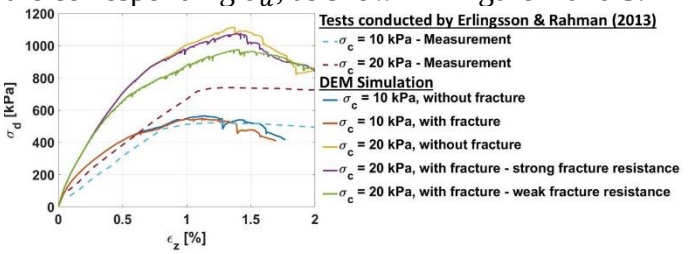

Figure 3. Deviatoric stress vs. axial strain of the loading head.

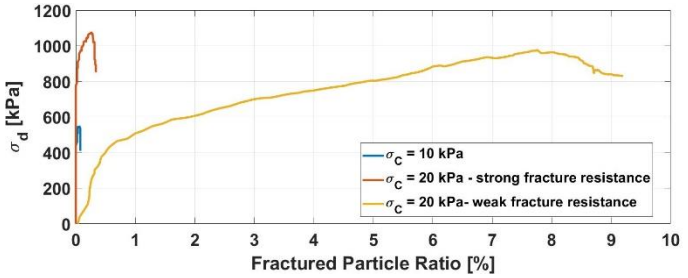

Figure 4. Fractured particle ratio vs. deviatoric stress.

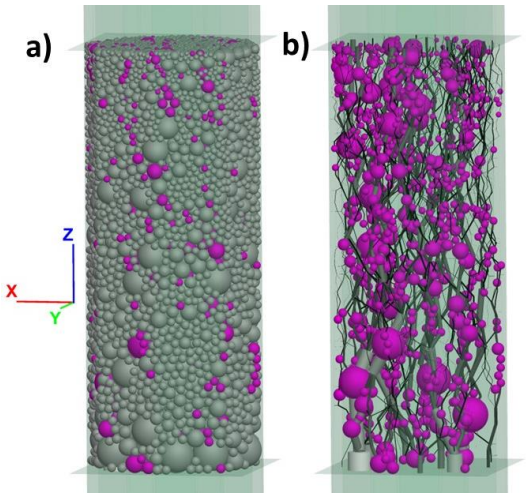

Figure 5. Distribution of fractured particles (pink) in UGM with weak aggregates, at σ_C = 20 kPa and maximum σ_d, a) particles, b) contact force skeleton.

In Figure 4, the ratio of fractured particles to the total number of particles is plotted for all confining cases. As observed, this ratio is relatively small for the cases of UGM with strong fracture resistance at the maximum σ_d. However, it increases to approximately 8% for the UGM with weak fracture resistance at maximum σ_d. A drastic increase in particle fracture can be observed for UGM with weak and strong fracture resistance at σ_d > 500 kPa, and σ_d > 900 kPa for at σ_C = 20kPa, respectively. The fractured particles within UGM and the location of fractured particles along with the contact force skeleton are shown in Figures 5a and 5b, respectively. The fractured particles are shown in pink colors, while the contact forces are represented in gray scale, with the lighter colors indicating stronger contact forces and the dark colors indicating weaker forces. It can be observed that fractured particles are evenly distributed within the UGM. This is to be expected, as the contact forces are evenly distributed throughout the UGM.

5 CONCLUSION

DEM study of the influence of aggregate fracture on the UGM response in monotonic triaxial tests is conducted. The modelling results are found to exhibit good qualitative and reasonable quantitative agreement with the experimental results from the literature.

The results from the DEM models demonstrate that particle fracture noticeably affects the maximum deviatoric stress that can be achieved at two confining pressure levels investigated. Additionally, the DEM model allows tracking the accumulation of particle fractures as a function of applied load, providing insights on both the location and the quantity of fractured particles. DEM modelling can thus serve as a valuable tool for investigating the performance of the materials with distinct properties, such as marginal road materials, under triaxial testing. Regarding the evaluation of unbound materials containing marginal aggregates, it should be noted that these aggregates may exhibit greater shape variation compared to standard aggregates. Consequently, the effect of aggregate shape will be explored in future studies, for example, by incorporating clumps in DEM to represent non-spherical particles.

6 REFERENCES

Cervera, C. C., Jelagin, D., Partl, M. & Larsson, P.-L., 2017. Contact-induced deformation and damage of rocks used in pavement materials. *Mater. Des.*, 133, pp. 255-265.

de Bono, J. P. & McDowell, G. R., 2014. DEM of triaxial tests on crushable sand. *Granular Matter*, 16, pp. 551-562.

Erlingsson, S. & Rahman, M. S., 2013. Evaluation of Permanent Deformation Characteristics of Unbound Granular Materials by Means of Multistage Repeated-Load Triaxial Tests. *Transportation Research Record*, 2369(1), pp. 11-19.

Etikan, M. K., Jelagin, D., Olsson, E. & Partl, M. N., 2024. Experimental and Numerical Analysis of Crushing Resistance of Unbound Road Materials. *International Journal of Pavement Engineering*, 25(1), p. 2330630.

Itasca Consulting Group Inc., 2019. PFC3D (particle flow code in 3 dimensions) version 6.0, Minneapolis.

Olsson, E., Jelagin, D. & Forquin, P. A., 2019a. Computational framework for analysis of contact-induced damage in brittle rocks. *Int. J. Solids Struct.*, 167, pp. 24-35.

Saeed, A., Barker, W. & Hall Jr., J. W., 2001. Performance-related tests of aggregates for use in unbound pavement layers, NCHRP Report. Washington: National Academy Press.

Yideti, T., Birgisson, B., Jelagin, D. & Guarin, A., 2013. Packing theory-based framework to evaluate permanent deformation of unbound granular materials. *International Journal of Pavement Engineering*, 14(3), pp. 309-320.

Zhang, H.-L., Tang, Y., Meng, T. & Zhan, L.-T., 2021. Evaluating the crushing characteristics of recycled construction and demolition waste for use in road bases. *Transp. Geotech.*, 28.